

Anomalous Chiral Behavior in Quenched Lattice QCD

W. Bardeen¹, A. Duncan², E. Eichten¹, and H. Thacker³

¹Fermilab, P.O. Box 500, Batavia, IL 60510

²Dept. of Physics and Astronomy, Univ. of Pittsburgh, Pittsburgh, PA 15260

³Dept. of Physics, University of Virginia, Charlottesville, VA 22901

Abstract

A study of the chiral behavior of pseudoscalar masses and decay constants is carried out in quenched lattice QCD with Wilson fermions. Using the modified quenched approximation (MQA) to cure the exceptional configuration problem, accurate results are obtained for pion masses as low as ≈ 200 MeV. The anomalous chiral log effect associated with quenched η' loops is studied in both the relation between m_π^2 vs. m_q and in the light-mass behavior of the pseudoscalar and axial vector matrix elements. The size of these effects agrees quantitatively with a direct measurement of the η' hairpin graph, as well as with a measurement of the topological susceptibility, thus providing several independent and quantitatively consistent determinations of the quenched chiral log parameter δ . For $\beta = 5.7$ with clover-improved fermions ($C_{sw} = 1.57$) all results are consistent with $\delta = 0.065 \pm 0.013$.

1 Introduction

Until recently, efforts to study the chiral limit of lattice QCD with Wilson-Dirac fermions have been impeded by the large non-gaussian fluctuations encountered at light quark mass (the “exceptional configuration” problem). These statistical problems have been shown to be symptomatic of the nonconvergence of the quenched lattice Monte Carlo integration due to the presence of exactly real Dirac eigenmodes in the physical mass region [1]. These real eigenmodes are of topological origin but are displaced from zero mass by the explicit chiral symmetry breaking of the Wilson-Dirac operator. The modified quenched approximation (MQA) is a prescription for constructing a modified quark propagator by shifting positive mass real poles to zero mass in a compensated way.[2] This procedure is the most straightforward and effective way of removing the lattice artifact which produces exceptional configurations while leaving the results for heavier quarks outside the pole region essentially unchanged. In the continuum limit, the spread of eigenmodes to positive mass shrinks to zero, so that if we shift all poles above a given quark mass, the fraction of gauge configurations in an ensemble that would require MQA pole-shifting approaches zero in the continuum limit. In this sense, the MQA has the right continuum limit, and provides a sensible definition of the otherwise undefined quenched theory at finite lattice spacing and small quark mass. Exactly how effective the MQA is in restoring the chiral behavior expected from quenched continuum arguments is a question that can best be addressed by detailed calculations. As we will show in this paper, by using the MQA procedure we are able to study the behavior of pseudoscalar masses and decay constants with high statistics down to much lower pion mass (ca. 200 MeV) than has previously been accessible at $\beta = 5.7$ (for example, a recent high statistics study [3] of quenched chiral behavior extends only to $m_\pi \approx 300$ MeV). The results confirm in considerable detail the expected chiral behavior predicted for these quantities from chiral Lagrangian arguments. The overall size of the

quenched chiral log parameter δ is about a factor of two smaller than the $\delta \approx 0.17$ expected from the theoretical result

$$\delta = \frac{m_0^2}{16\pi^2 f_\pi^2 N_f}, \quad (1)$$

using the physical values of $m_{\eta'}$ and f_π . (Here the normalization of f_π is such that its physical value is ≈ 95 MeV. Chiral perturbation theory and the physical mass of the η' give $m_0 \approx 850$ MeV.) Nevertheless, the quantitative relations between various quantities inferred from continuum chiral Lagrangian arguments appear to be well-satisfied. In fact, the smallness of δ is consistent with our previous calculations at heavier quark mass which did not use MQA shifting [4].

In this paper, we describe several independent quantitative estimates of the quenched chiral log (QCL) parameter δ : (1) a direct measurement of the η' hairpin diagram, (2) a calculation of the topological susceptibility combined with the Witten-Veneziano formula [5], (3) measurement of the QCL effect in m_π^2 vs. m_q and in the vacuum-to-one-particle matrix element of the pseudoscalar density, (4) by fitting cross-ratios of masses and matrix elements using the lowest order chiral perturbation theory prediction (to first order in δ), and (5) by a global fit of all masses and matrix elements to the next-to-leading order chiral perturbation theory prediction. When the two quark masses in the pion are allowed to vary independently, as in (4) and (5), the corresponding masses and decay constants provide additional tests of quenched chiral log structure (c.f. the analysis of the CPPACS collaboration[3]). In this paper we present the results of analyses of chiral log structure both in the “diagonal” (equal quark mass) sector, and for mesons with unequal quark masses. The various determinations of δ are all consistent within statistics, giving an exponent $\delta = .065(13)$ for clover-improved Wilson fermion action, and $\delta = .06(2)$ for unimproved Wilson.

As discussed below, operators which do not change chirality, such as the axial-vector

current, are not expected to exhibit any QCL singularity (for equal mass quarks). In agreement with this theoretical expectation, our results for the mass dependence of the axial-vector decay constant show smooth analytic behavior with no enhancement in the chiral limit. The contrast between the singular chiral behavior of the pseudoscalar matrix element and the smooth analytic behavior of the axial-vector matrix element is a particularly convincing piece of evidence that we are indeed seeing the effects of virtual η' loops.

In Section 2 we briefly review the essential features of quenched chiral behavior in QCD in the language of effective field theory. Details of the lattice calculations are presented in Section 3. The direct determinations of δ from the η' hairpin correlator and from the topological susceptibility are presented in Section 4. In Section 5, QCL effects in the squared pseudoscalar mass as a function of quark mass are discussed, for “diagonal” mesons composed of equal mass quarks only. The QCL behavior of the pseudoscalar and axial-vector decay constants (again, for diagonal mesons only) is studied in Section 6. In Section 7 we extract the chiral log parameter δ from an analysis of cross-ratios of pseudoscalar meson masses and decay constants, along the lines of the CPPACS analysis [3]. In Section 8 we compare our lattice data for all mesons (equal and unequal quark masses) with the results of a detailed quenched chiral perturbation theory (to order p^4) calculation for the pseudoscalar masses and decay constants. Finally, in Section 9 we summarize our results and draw some broad conclusions. Some technical remarks on the efficacy and accuracy of the all-source technique used to extract hairpin amplitudes are relegated to Appendix 1, while chiral perturbation theory formulas for pseudoscalar and axial decay constants are given in Appendix 2.

2 Brief review of quenched chiral theory

The presence of anomalous chiral behavior induced by the quenched approximation was first investigated in the work of Sharpe [6] and Bernard and Goltermann [7]. Physically, the quenched chiral log effect can be understood as a consequence of the absence of topological screening in quenched QCD. Diagrammatically, the quenched approximation discards some, but not all, of the η' hairpin mass insertions. Instead of the massive η' propagator of full QCD, the quenched hairpin diagram exhibits a double Goldstone pole, see Fig[1]. This leads to infrared singular η' loop diagrams, such as that shown in Fig[2]. which alter the chiral behavior of certain matrix elements. A convenient way to understand the effect of the QCL singularities is to interpret them as a renormalization factor in the chiral field. Begin with a $U(3) \times U(3)$ chiral Lagrangian with a chiral field

$$U = \exp \left[i \sum_{i=0}^8 \lambda_i \pi_i / f \right] \equiv e^{i\pi_0/f} \tilde{U} \quad (2)$$

where $\lambda_0 = 1$ and $\pi_0 \equiv \eta'$ represents the $SU(3)$ -flavor singlet meson. Now consider the effect of integrating out the η' field. The remaining $SU(3) \times SU(3)$ Goldstone fields will be renormalized

$$U \rightarrow \langle e^{i\pi_0/f} \rangle \tilde{U} = \exp \left[-\langle \pi_0^2 \rangle / 2f^2 \right] \tilde{U} \quad (3)$$

where, in the quenched theory,

$$\langle \pi_0^2 \rangle = \int \frac{d^4 p}{(2\pi)^4} \frac{1}{p^2 + M_{\eta'}^2} \rightarrow \int \frac{d^4 p}{(2\pi)^4} \frac{-m_0^2}{(p^2 + M_{\pi}^2)^2} \quad (4)$$

In full QCD, the η' mass is large, so the effect of integrating out the η' field is to induce a finite renormalization that is nonsingular in the chiral limit. The chiral limit is described by the $SU(3) \times SU(3)$ chiral Lagrangian without an η' . Now consider the effect of quenching on the result of integrating out the η' field. The double Goldstone pole in the quenched η'

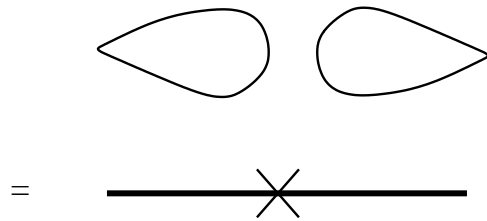


Figure 1: Chiral Lagrangian representation of the quark hairpin diagram as an η' mass insertion.

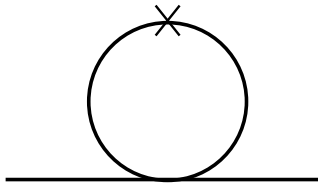


Figure 2: A quenched η' loop diagram which produces anomalous chiral log behavior.

propagator produces logarithmically divergent loop integrals in chiral perturbation theory. This results in a renormalization factor for the field U that is singular in the chiral limit, and thus alters the $m_\pi \rightarrow 0$ behavior of the chiral field:

$$U \rightarrow \exp \left[-\delta \log m_\pi^2 \right] \tilde{U} = \left(\frac{1}{m_\pi^2} \right)^\delta \tilde{U} \quad (5)$$

where \tilde{U} is nonsingular as $m_\pi \rightarrow 0$. In the following subsections, we will discuss the chiral log effect (or lack thereof) in the pseudoscalar and axial-vector charge matrix elements and in the mass of the pion as a function of quark mass.

Define the decay constants f_P and f_A

$$\begin{aligned} \langle 0 | \bar{\psi} \gamma^5 \psi | \pi(p) \rangle &= f_P \\ \langle 0 | \bar{\psi} \gamma^5 \gamma^\mu \psi | \pi(p) \rangle &= p^\mu f_A \end{aligned} \quad (6)$$

From the chiral-field expressions for the quark bilinears,

$$\begin{aligned} \bar{\psi} \gamma^5 \psi &\propto U - U^\dagger \\ \bar{\psi} \gamma^5 \gamma^\mu \psi &\propto i \left(U^{-1} \partial^\mu U - (\partial^\mu U^{-1}) U \right) , \end{aligned} \quad (7)$$

we conclude that a singular chiral log factor will appear in the quenched calculation of f_P , but not of f_A ,

$$\begin{aligned} f_P^{\text{quenched}} &= \left(\frac{1}{m_\pi^2} \right)^\delta \tilde{f}_P \\ f_A^{\text{quenched}} &= \tilde{f}_A \end{aligned} \quad (8)$$

where \tilde{f}_P and \tilde{f}_A go to a constant in the chiral limit. Both of these expectations are confirmed by the data, as discussed below. The chiral behavior of the pion mass as a function of quark mass is easily derived from the results for the pseudoscalar and axial-vector densities, combined with PCAC. This gives

$$m_\pi^2 \simeq \text{const.} \times m_q \times \left(\frac{1}{m_\pi^2} \right)^\delta, \quad m_q \rightarrow 0 \quad (9)$$

This predicted behavior is also confirmed by the lattice results, as discussed in Section 5.

The quantitative significance of the quenched chiral log behavior that we observe is further reinforced by comparing it with a direct calculation of the anomalous exponent δ . We have done this calculation in two related but distinct ways. One is a calculation of the hairpin diagram Fig[1].

$$\Delta_h(x) = \langle \text{Tr} \gamma^5 G(x, x) \text{Tr} \gamma^5 G(0, 0) \rangle \quad (10)$$

where $G(x, y)$ is the quark propagator. The size of the hairpin mass insertion determines the coefficient of the logarithmic divergence in the η' loop diagrams. Let us denote by m_0^2 the value of the η' mass insertion vertex obtained from the long-range behavior of the hairpin diagram. Then the predicted chiral log exponent is given by Equation (1).

The other quantity which provides an evaluation of δ is the topological susceptibility, χ_t . The Witten-Veneziano formula allows us to relate χ_t to the η' mass insertion,

$$m_0^2 = \frac{2N_f}{f_\pi^2} \chi_t \quad (11)$$

where N_f is the number of (light) quark flavors. The topological susceptibility is given in terms of winding numbers ν on a lattice of four-volume V by

$$\chi_t = \frac{\langle \nu^2 \rangle}{V} \quad (12)$$

To calculate winding numbers, we use the integrated anomaly technique (“fermionic method”) of Smit and Vink [8]. The configuration-by-configuration calculation of winding numbers provides a determination of the χ_t , and hence via (11) and (1), an estimate of δ . The results obtained from the hairpin residue and from the topological susceptibility are in good agreement for clover improved fermions, as discussed in Section 4.

3 Lattice calculation of pseudoscalar masses and decay constants

Most of the results which we will focus on in the subsequent discussion are obtained from the “b” ensemble of gauge configurations from the Fermilab ACPMAPS library. This ensemble consists of a set of 300 quenched configurations on a $12^3 \times 24$ lattice at $\beta = 5.7$. The fermion action used in our calculations was clover improved with a clover coefficient of $C_{sw} = 1.57$. To get some estimate of lattice spacing effects and finite volume corrections, we also calculated masses and decay constants on 200 configurations of the b-lattice ensemble with unimproved Wilson fermions ($C_{sw} = 0$), and on the a-lattice ensemble ($16^3 \times 32$ at $\beta = 5.7$), also with unimproved Wilson fermions. The masses and decay constants and their quoted errors are obtained from fully correlated fits to the smeared-smeared and smeared-local propagators, using a smeared pseudoscalar source in Coulomb gauge combined with local pseudoscalar and axial-vector sources. Calculations with different smearing functions give results that are consistent within less than one standard deviation, indicating that the systematic error associated with excited state contamination is less than our statistical errors. For the hairpin correlator, the issue of excited state contamination is addressed in detail in Section 3.2 by comparing the ratio of smeared and local hairpin propagators. Remarkably, we find that for small quark masses there is very little excited state contribution to the hairpin propagator, even at time separations as small as $t = 1$. This is in marked contrast to the valence pion propagator, which has substantial excited state components at short time. We conclude that the hairpin vertex itself is largely decoupled from the excited states in the pseudoscalar channel.

The essential new ingredient in the present study which allows a detailed exploration of chiral behavior is the use of the pole-shifting procedure of the modified quenched ap-

proximation. The details of this procedure and its effectiveness in resolving the exceptional configuration problem have been described previously [2]. For each gauge ensemble and choice of fermion action, we carried out a careful scan of each configuration for poles over a range of quark masses, starting at a value heavy enough to be beyond all real eigenmode poles and going to nearly zero mass. For example, in the run with clover action, where $\kappa_c = 0.14329$, poles appeared as low as $\kappa \approx 0.1417$ ($m_q \simeq 45$ MeV), and we scanned for and located all poles up to 0.1431. The value of the integrated pseudoscalar charge $Q_5 = \int d^4x \bar{\psi} \gamma^5 \psi$ is calculated for a sequence of hopping parameter values, using the same allsource method that is used to calculate the hairpin propagator (see below). A Pade fit to these Q_5 values determines the location of any poles within and somewhat beyond the range scanned. Extremely precise pole locations can be obtained by performing further conjugate gradient inversions very close to the pole positions determined by the Pade fit. Using the stabilized biconjugate gradient algorithm, we are able to perform inversions at hopping parameters very close to the pole position without any major increase in convergence time. In our calculations, we have located the pole positions as a function of hopping parameter κ to at least 8-digit accuracy in all cases. Once all the visible poles in an ensemble are located, their residues in the quark propagator are determined by performing inversions slightly above and below the pole and subtracting. We found that accurate pole residues could be computed for a pole at κ_0 by inverting at $\kappa = \kappa_0 \pm .000001$. (The computation of pole residues can be done very economically by noting that the pole contribution to all 12 color-spin components of the quark propagator can be obtained from a single color-spin inversion above and below the pole, i.e. only 1/12 of a full propagator calculation is required.)

An alternative procedure for locating poles of the quark propagator $\propto 1/(\not{D} - m_q)$ is to use the Arnoldi algorithm [9] to partially diagonalize the Wilson-Dirac operator in the region around zero mass. The returned eigenvalues are the pole positions, and the residues needed

to perform the pole-shifting procedure may be reconstructed from the Arnoldi eigenvectors. This method locates not only the real eigenvalues but also the complex ones in the continuum band. The Arnoldi analysis has been carried out [10] on a subset of the configurations used in this investigation, extracting approximately 50 eigenvalues from each gauge configuration analyzed. For the lattices which exhibited visible poles in the bicongradstab scanning procedure described above, the results of the Arnoldi calculation agree accurately with that analysis for both the pole positions and residues. The low-lying spectrum for an “exceptional” gauge configuration ($b : 021000$) is shown in Fig[3]. (Note: The positive mass region is to the right in this plot. The three modes farthest to the right on the real axis were MQA shifted.)

The effect of the MQA pole-shifting procedure is to eliminate the problem of exceptional configurations and to dramatically improve error bars on all quantities calculated from light quark propagators, as shown in detail in Ref.[2]. Since the η' hairpin propagator is particularly sensitive to the topological structure of gauge configurations, the improvement obtained by using the MQA for the hairpin calculations is even more striking than that for valence-quark meson propagators. The MQA-improved results are sufficiently accurate to allow a detailed study of the time-dependence of the hairpin propagator even as far out as $t = 9$ or 10 . Over the entire time range starting from $t = 1$, this time-dependence is in reasonably good agreement with that predicted from a pure double pion pole form. The lack of any significant single-pole contribution to the hairpin propagator is consistent with the absence of excited states. (A heavy excited state on one side of the hairpin vertex would produce an effective single pion pole term.) A single-pole term in the time-dependence could also arise from a p^2 -dependent hairpin vertex. In the chiral Lagrangian, this would correspond to a renormalization of the η' kinetic term in addition to a mass insertion. The fact that the time-dependence of the hairpin correlator is well-described by the pure double

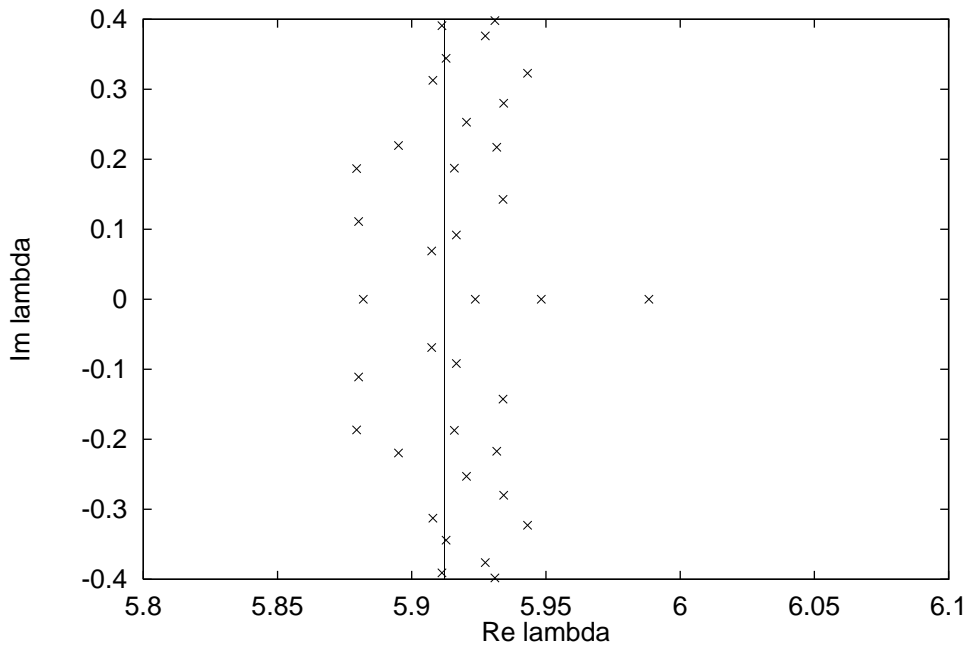


Figure 3: A portion of the low-lying spectrum of the $C_{sw} = 0$ Wilson-Dirac spectrum of a quenched gauge configuration (b_021000 of the ACPMAPS library) in the region $\lambda \approx 1/\kappa_c$. This configuration has four real poles in the continuum band. The vertical line is at $Re \lambda = 1/\kappa_c$. The three real poles farthest to the right on the plot require shifting.

pion pole form over the entire time range from $t = 1$ to 12 lends quantitative support to the assumption, often used in phenomenological discussions, that the momentum dependence is mild and the η' hairpin can therefore be treated simply as a mass insertion. The time-dependence is discussed in more detail in Section 4.2. The final results quoted for the mass insertion value m_0^2 are obtained from a 1-parameter fit of the hairpin to a pure double-pole formula, with the pion mass held fixed at the value obtained from the corresponding valence pion propagator.

4 The η' mass and the chiral log parameter δ

4.1 Topological susceptibility

For both the hairpin correlator and the calculation of the integrated pseudoscalar charge Q_5 , the method used is one introduced into such loop calculations in Ref.[11]. This method employs an “allsource” quark propagator calculated with a source that consists of a color-spin unit vector on *all sites* of the lattice. This allows closed quark loops originating from any space-time point to be included in a calculation (e.g. of $Q_5 = TrG\gamma^5$ or of a hairpin diagram), relying on random gauge phases to cancel out the gauge-variant open loops. Even on a single gauge configuration, this method is a reasonably accurate way of calculating global quantities like Q_5 , since random phase cancellation of noninvariant terms should take place in the sum over sites. The topological winding number ν of each gauge configuration can be determined using the integrated anomaly equation [8],

$$\nu = -im_q Q_5 \tag{13}$$

Thus we expect the quark-mass dependence of Q_5 to exhibit a simple pole at $m_q = 0$ with residue given by the winding number. The plots of Q_5 vs. m_q for two typical configurations (after MQA pole shifting) are shown in Fig[4]. The solid line in each case is the best single-pole fit. For the 300 lattice ensemble with clover action, the distribution of winding numbers determined in this way is shown in Fig[5].

The topological susceptibility χ_t can now be calculated as the mean squared winding number per unit four-volume

$$\chi_t = \frac{\langle \nu^2 \rangle}{V} = \frac{m_q^2}{V} \langle Q_5^2 \rangle \tag{14}$$

By calculating the last expression in (14) we observe only a slight quark-mass dependence of

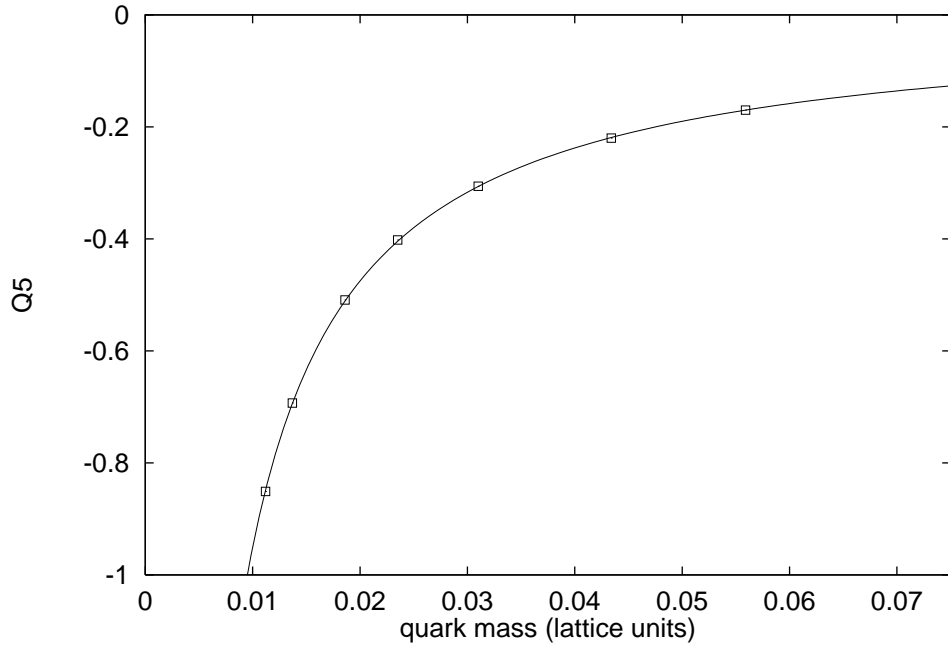
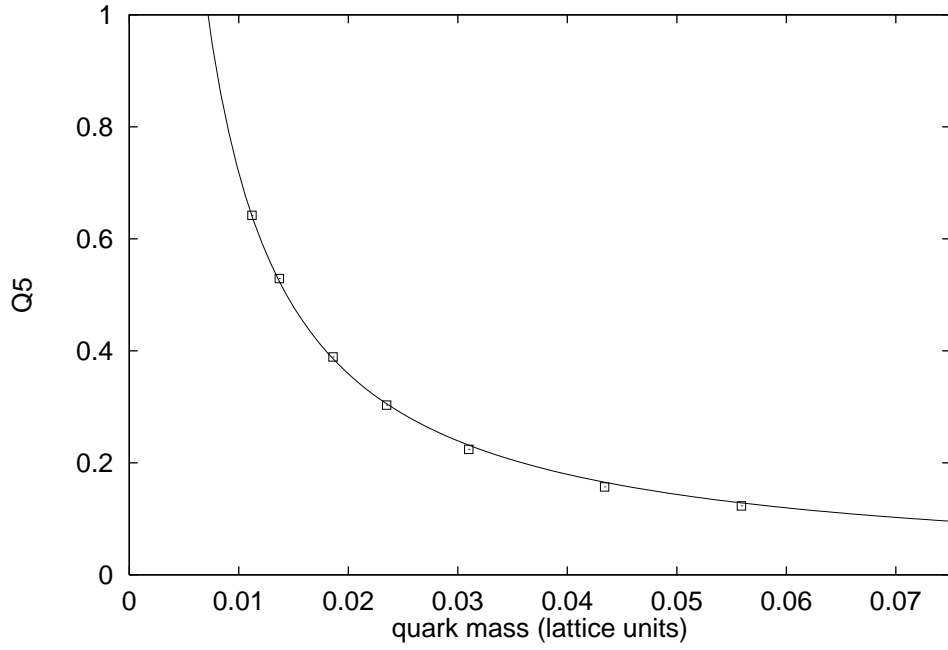


Figure 4: Q_5 as a function of quark mass for two typical gauge configurations after MQA pole shifting.

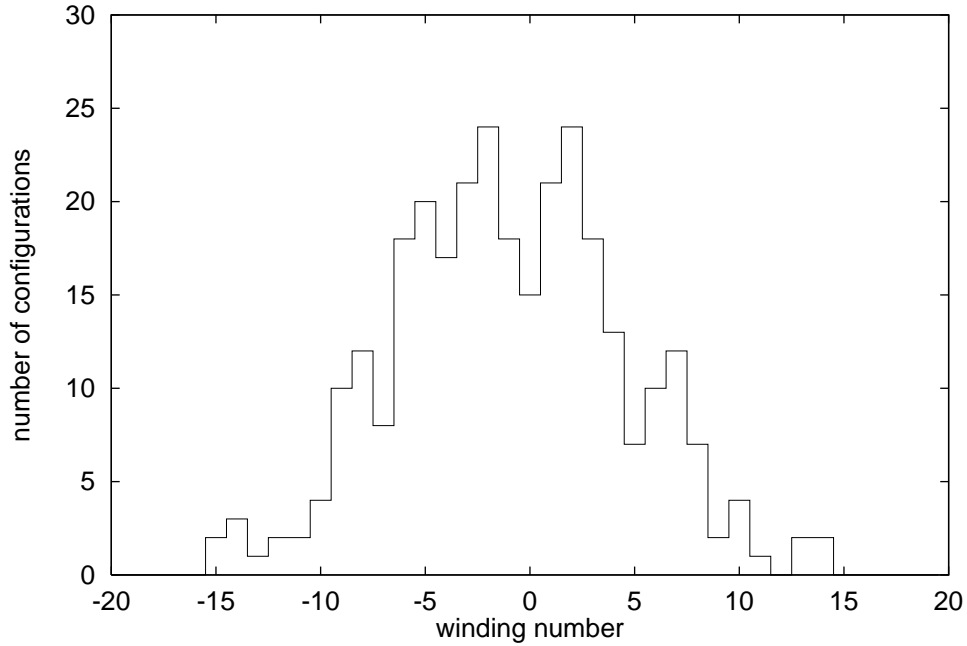


Figure 5: The distribution of winding numbers determined from the integrated pseudoscalar density.

the result, as shown in Fig[6]. Extrapolating to the chiral limit, we obtain, for $C_{sw} = 1.57$,

$$\chi_t = 6.48(58) \times 10^{-4} = (188 \text{ MeV})^4 \quad (15)$$

where the first result is in lattice units, and the second is obtained by using the charmonium scale at $\beta = 5.7$ of $a^{-1} = 1.18 \text{ GeV}$. The corresponding result for unimproved Wilson fermions ($C_{sw} = 0$) is

$$\chi_t = 3.24(39) \times 10^{-4} = (158 \text{ MeV})^4 \quad (16)$$

Using the topological susceptibility and the value of axial vector decay constant obtained from the valence propagator fits (see Section 6), the Witten-Veneziano formula gives

$$\delta = .063(6) \quad (17)$$

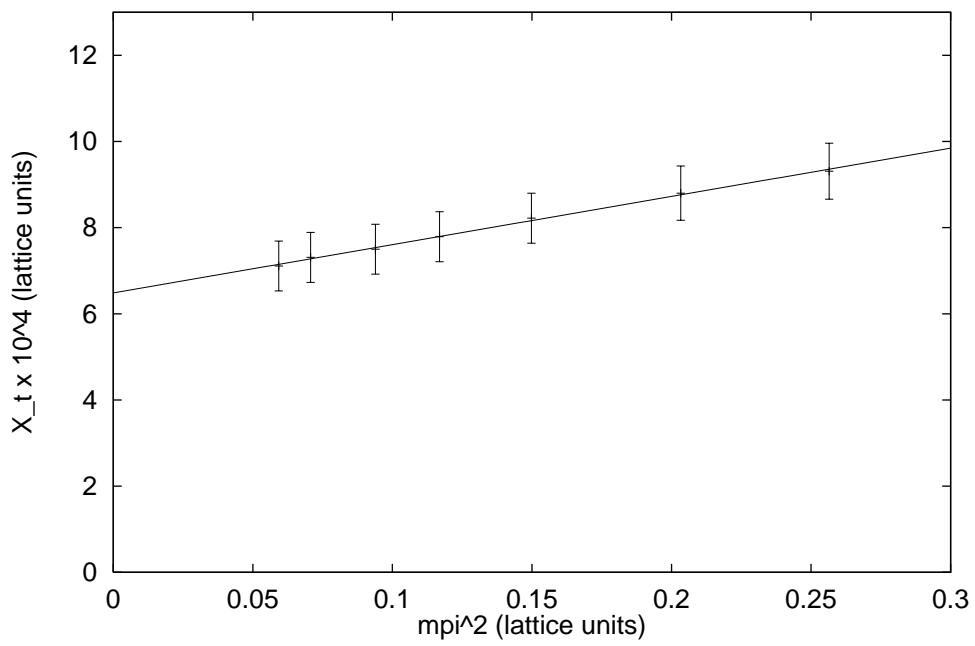


Figure 6: Topological susceptibility calculated by the fermionic method on a $12^3 \times 24$ lattice with clover improved ($C_{sw} = 1.57$) fermions as a function of the quark mass used to determine Q_5 .

for clover improved quarks ($C_{sw} = 1.57$), and

$$\delta = .074(9) \tag{18}$$

for unimproved Wilson quarks. In (17) and (18) we used the bare quark mass obtained from the hopping parameter to determine winding numbers from Q_5 values. Here and elsewhere, we have taken the bare quark mass to be the pole mass

$$m_q = \log \left(1 + \frac{1}{2}(\kappa^{-1} - \kappa_c^{-1}) \right) \tag{19}$$

but the results for the chiral log parameter are not significantly different if we use the naive bare mass $(\kappa^{-1} - \kappa_c^{-1})/2$. If instead we use the current algebra mass

$$m_q^{CA} \equiv f_A m_\pi^2 / 2f_P, \tag{20}$$

the result (17) is essentially unchanged, while the $C_{sw} = 0$ result (18) is decreased to

$$\delta = .032(4) \tag{21}$$

(See discussion following Eq. (28).)

An important check on the calculation of topological susceptibility is to show that $\langle \nu^2 \rangle$ has the proper dependence on volume, i.e. $\langle \nu^2 \rangle \propto V$. In Fig[7] we compare the topological susceptibility calculated on a $12^3 \times 24$ lattice and on a $16^3 \times 32$ lattice, both with unimproved Wilson fermions ($C_{sw} = 0$). The results shown in Fig[7] are consistent with the expected extensive property, i.e. a linear volume dependence.

4.2 Hairpin correlator and the η' mass insertion

Using the same allsource propagators as in the previous subsection, we calculate the hairpin contribution to the flavor singlet pseudoscalar propagator, i.e. the loop-loop correlator (10). Earlier calculations of this correlator [11, 4, 12] were restricted to relatively heavy

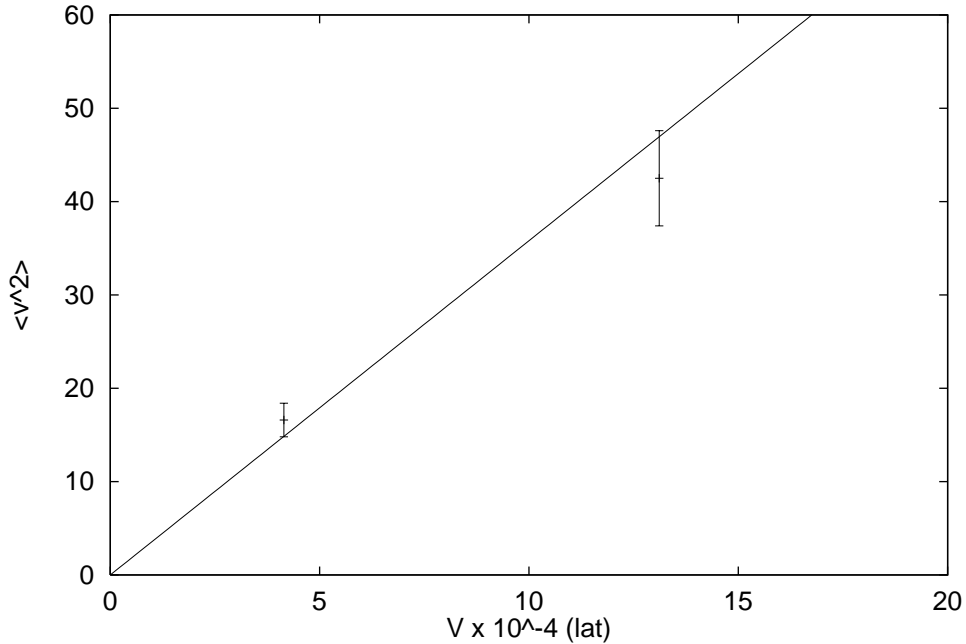


Figure 7: The volume dependence of $\langle \nu^2 \rangle$ for $12^3 \times 24$ and $16^3 \times 32$ lattices, for Wilson-Dirac fermions, $C_{sw} = 0$

quark mass and had large errors which prevented a detailed study of time-dependence. As discussed in the Introduction, the statistical problems encountered in these previous investigations arise from exactly real Wilson-Dirac eigenmodes, the effect of which is magnified by the fact that the hairpin propagator receives its largest contributions from topologically nontrivial gauge configurations which necessarily contain such real modes. The MQA pole-shifting procedure is thus particularly effective in improving the hairpin calculation. Fig[8] shows an example of a hairpin propagator before and after MQA improvement of the corresponding quark propagators. The quark mass is still rather heavy here ($m_q \simeq 36$ MeV, $m_\pi = .386a^{-1} \approx 450$ MeV). For even lighter quarks, the unimproved hairpin propagator is unmeasurable, with errors $> 100\%$, while the MQA improved hairpin is still quite well determined, allowing a reasonably accurate measurement of the η' mass insertion even at the lightest quark mass we have studied.

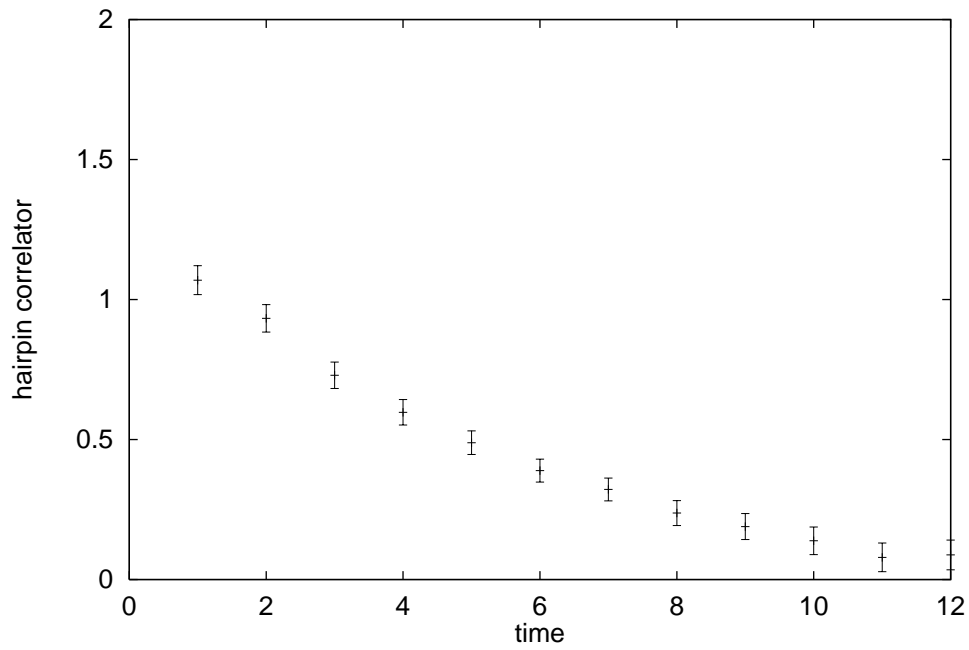
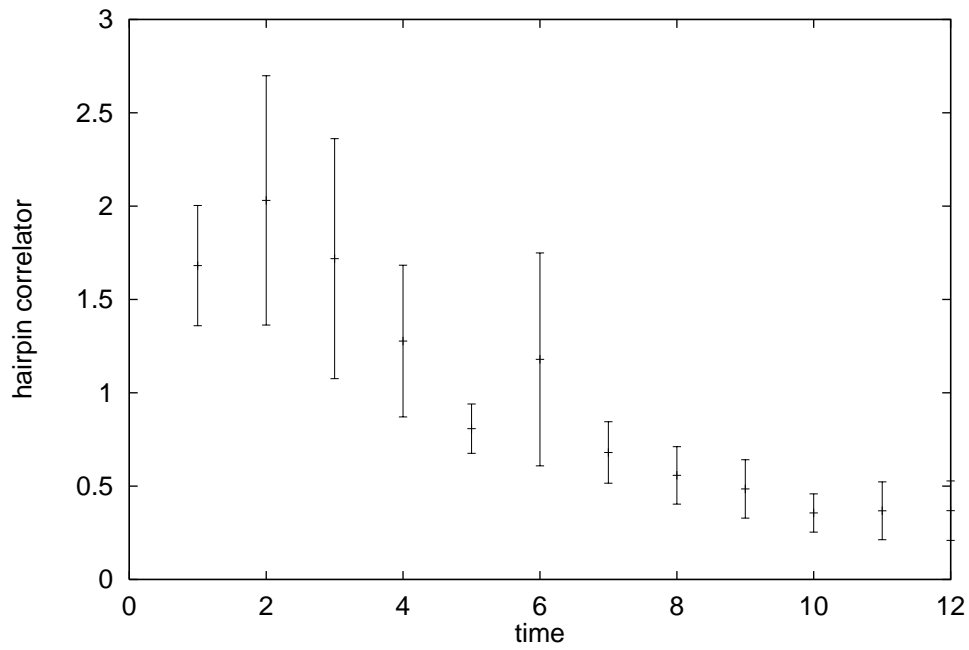


Figure 8: The hairpin correlator for $\kappa = .1420$, $C_{sw} = 1.57$ before and after MQA improvement.

The size and time-dependence of the hairpin correlator is measured accurately enough in the MQA method to address the two issues of excited state contamination and p^2 -dependent vertex insertion terms mentioned in the Introduction. These two effects are distinct, but they are difficult to disentangle from the time-dependence alone, since they both have the effect of adding a single pole term to the correlator. Fortunately, there is another way to determine the presence or absence of excited states, namely, to study the ratio of hairpin correlators obtained from smeared and local $\bar{\psi}\gamma^5\psi$ sources. This can be compared with the overlap of the same smeared and local sources with the ground-state pion, as determined from the large- t behavior of the corresponding valence pion propagators.

We construct smeared-source hairpin correlators by a modification of the allsource method used for the local-source hairpins. In the latter, the source used for propagator inversion was a unit color-spin vector on every site. In order to obtain meaningful results for smeared source propagators, we must perform the smearing in Coulomb gauge. The smeared sources used for the valence pion propagators were constructed using an exponential smearing function $\propto e^{-\lambda r}$. Based on other studies of hadron wave functions at this value of β , we took $\lambda = 0.5$ in lattice units. There is an additional subtlety in the implementation of Coulomb gauge smearing in the allsource method. Since this method relies on random gauge phase cancellations, the actual sums over sites for the two ends of the hairpin must be carried out in the original unfixed gauge. In fact we carry out all calculations in the unfixed gauge, just as in the local calculation. The only difference is that the source used for propagator inversion is a “smeared allsource” which is constructed by the following procedure:

1. Construct an ordinary allsource, i.e. a unit color-spin vector on every site.
2. To the allsource, apply the gauge transformation that transforms from the original unfixed gauge to the Coulomb gauge.

3. Smear the source terms on each site in Coulomb gauge by convoluting with an exponential smearing function. (This is most efficiently done in momentum space using FFT's.)
4. Transform the smeared allsource back to the original unfixed gauge.

This smeared allsource can be used as the source for the quark propagator calculation, and the subsequent analysis is identical to that of the local hairpin correlator. In Coulomb gauge the smeared allsource is a superposition of real exponential sources originating from every point. By going back to the unfixed gauge, we attach a random SU(3) gauge phase to each exponential, so that a quark loop which starts on one exponential and ends on another will have a random phase (even if it actually starts and ends at the same space-time point), whereas terms which start and end on the same exponential have no random phase (even if they start and end on different points). In this sense, the method is very similar in spirit to one introduced earlier by Weingarten, et al [13], where multiple smeared sources are introduced in hadron spectroscopy calculations by attaching random U(1) phases to each source.

The ratio of ground-state overlaps of the smeared and local sources with the pion is easily and accurately determined from the behavior of the smeared-smeared and smeared-local valence pion propagators. As discussed in the next section, values for the pion mass and for the ground-state overlaps are obtained from a combined fit to the propagators using smeared pseudoscalar, local pseudoscalar, and local axial vector sources and sinks.

Define the local and smeared $\bar{\psi}\gamma^5\psi$ operators by $P_l(x)$ and $P_s(x)$ respectively, and measure the corresponding matrix elements,

$$\langle 0|P_i(0)|\pi(\vec{p}=0)\rangle = f_P^{(i)} \quad i = l, s \quad (22)$$

To test for the presence of excited states in the hairpin correlator, define the smeared and

local hairpin correlators (at zero 3-momentum) $\Delta_h^{(i)}(t)$, $i = s, l$ and plot the ratio

$$R(t) \equiv \frac{\Delta_h^{(l)}(t)/(f_P^{(l)})^2}{\Delta_h^{(s)}(t)/(f_P^{(s)})^2} \quad (23)$$

If there are no excited states, this ratio should be equal to unity. In Fig[9] we plot this ratio for one of the lightest mass hairpins calculated ($\kappa = .1427$ or $m_q = .0137$ in lattice units). The absence of any excited state contamination in the hairpin propagator is striking. By contrast, the ratio of valence propagators at small times is substantially larger than its asymptotic value, indicating that the local valence propagator has a larger excited state contribution. We conclude that the hairpin vertex is very nearly decoupled from excited pseudoscalar states. In Fig[10], we also plot the results of a similar analysis for a heavier quark mass ($k = .1410$ or $m_q = .0559$ in lattice units). Here the relative contribution of excited states to the valence propagator (also shown in the plot) is even larger than in the light mass case. The hairpin propagator, on the other hand, still exhibits little if any excited state contribution. For $t \geq 2$, there is no significant departure of the hairpin ratio from its asymptotic value. This analysis of the smeared-to-local hairpin ratio has been carried out at all the other mass values with similar conclusions. In no case is there any significant indication of excited states for $t \geq 2$.

The demonstrated absence of excited states from the hairpin diagram allows us to make effective use of the time-dependence of the correlator to investigate the structure of the hairpin vertex. The simplest assumption, often invoked in phenomenological discussions, is that the hairpin is simply a momentum independent mass insertion m_0^2 . With this assumption, the quenched hairpin correlator in momentum space is given by

$$\tilde{\Delta}_h(p) = f_P \frac{1}{p^2 + m_\pi^2} m_0^2 \frac{1}{p^2 + m_\pi^2} f_P \quad (24)$$

Fourier transforming over p_0 , this implies a time-dependence for the zero momentum prop-

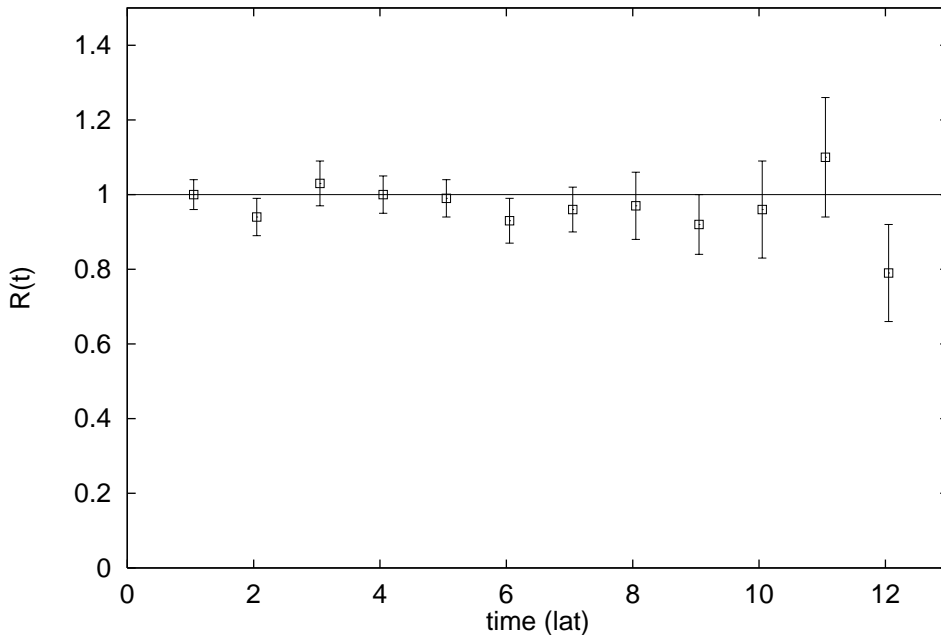


Figure 9: Ratio $R(t)$ of the local-source hairpin divided by the smeared-source hairpin with $\kappa = .1427$, normalized by the asymptotic valence propagator ratio.

agator of

$$\Delta_h(\vec{p} = 0; t) = \frac{f_P^2 m_0^2}{4m_\pi^3} (1 + m_\pi t) e^{-m_\pi t} + (t \rightarrow N_T - t) \quad (25)$$

This structureless hairpin vertex is suggested by large N_c arguments, but it is important to test for the more general possibility that the vertex has some additional p^2 dependence. To lowest order in a p^2 expansion, this would generalize the above analysis by the replacement

$$m_0^2 \rightarrow \Pi(p^2) \approx \Pi(-m_\pi^2) + (p^2 + m_\pi^2) \Pi'(-m_\pi^2) + \dots \quad (26)$$

To test for p^2 dependence of the hairpin vertex, and to estimate its effect on the determination of the η' mass, we carried out two sets of correlated fits to the hairpin time-dependence, one with the pure double-pole formula (25) and one to the single-pole + double-pole formula resulting from (26). In all these fits, the pion mass was held fixed at the value given by the valence propagator analysis. Since we have already demonstrated that there is

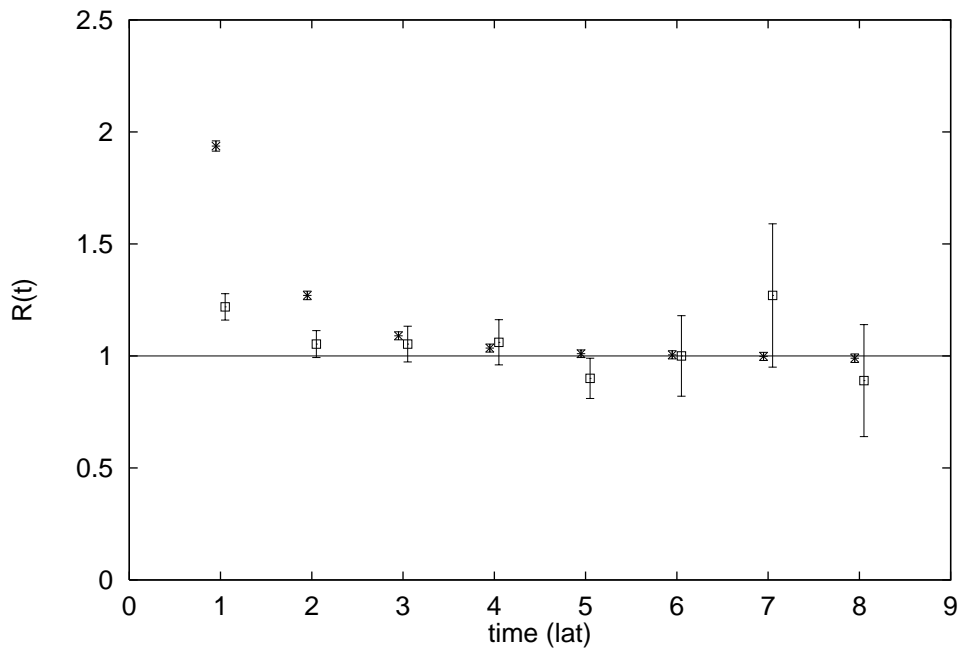


Figure 10: Ratio $R(t)$ (boxes) of the local-source hairpin divided by the smeared-source hairpin with $\kappa = .1410$, normalized by the asymptotic valence propagator ratio. Also shown (\times 's) is the same ratio for the valence propagator.

very little excited state contamination in the hairpin propagator, the range of times used in the fits is taken to be $2 \leq t \leq 10$. To summarize the overall results of these fits, the hairpin time dependence for all the quark masses studied is well described by a single-parameter fit to the pure double-pole formula (25). (Here the pion mass is not a fit parameter, since it is already accurately determined from the valence propagator.) In Fig[11] we show an example of a pure double pole fit to the hairpin correlator over the entire accessible t range. We conclude that the hairpin vertex is reasonably well described by a momentum-independent mass insertion. The final results for m_0^2 , given in Table 1, are extracted from pure double pole fits. Using Equation (1) and the lattice value for $f_\pi (= f_A/\sqrt{2})$ (see Table 2), this gives

$$\delta = .062(7) \tag{27}$$

for $C_{sw} = 1.57$, and

$$\delta = .044(5) \tag{28}$$

for $C_{sw} = 0$. Note that, in the pure double-pole approximation to the hairpin correlator, the value of δ from χ_t and that obtained from the hairpin residue are related by a factor $(f_A m_\pi^2 / 2 f_P m_q)^2$, which should be unity by the chiral Ward identity. The agreement between (17) and (27) for the clover-improved calculations can be traced to the following two facts: (1) The double-pole formula gives a good description of the hairpin correlator for all time separations, and (2) The Ward identity is well-satisfied for $C_{sw} = 1.57$. (By contrast, the current algebra quark mass is about 40% smaller than the bare mass for $C_{sw} = 0$.)

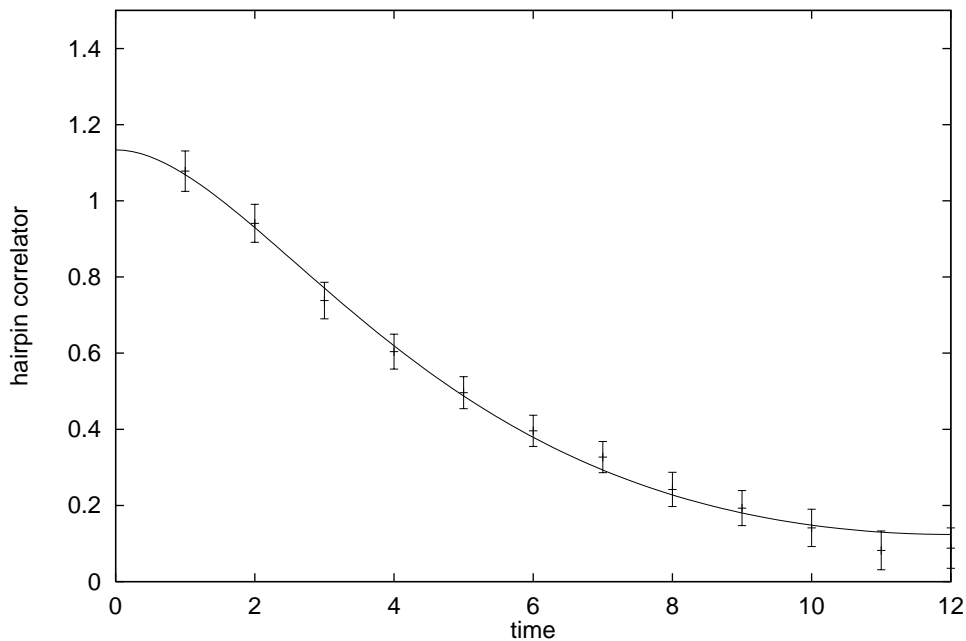


Figure 11: One-parameter fit to a pure double-Goldstone pole form for the hairpin correlator at $\kappa = .1420$. Pion mass is fixed from the valence propagator analysis.

Table 1: Value of m_0 , the hairpin contribution to the η' mass, for $C_{sw} = 1.57$ (first two columns) and $C_{sw} = 0$ (last two columns) at $\beta = 5.7$, for $N_f=3$.

κ	$m_0 a$	κ	$m_0 a$
.1410	.517(23)		
.1415	.534(24)	.1630	.179(10)
.1420	.554(24)	.1650	.239(16)
.1423	.568(26)	.1667	.289(13)
.1425	.576(27)	.1675	.321(13)
.1427	.576(30)	.1680	.338(13)
.1428	.576(33)	.1685	.353(18)
κ_c	.580(27)	κ_c	.393(15)

5 Quenched chiral logs in the pseudoscalar mass

The effect of quenched η' loops on the chiral behavior of the pseudoscalar mass is one of the most definitive predictions of the quenched chiral log analysis.[6, 7] In a previous analysis of the pion mass as a function of quark mass,[4] no evidence was found for quenched chiral log behavior at $\beta = 5.7$ for unimproved Wilson fermions, with a one-standard-deviation upper bound on the chiral log parameter of $\delta < .07$. This was also shown to be consistent with the size of the hairpin propagator. That analysis was done before the development of the MQA method for resolving the exceptional configuration problem, and the lightest pion mass used was $m_\pi a = .253$ (hopping parameter $\kappa = .1680$ and $C_{sw} = 0$). With MQA improvement of quark propagators we obtain much better statistical errors on m_π and also are able to go to a much lighter quark mass ($m_\pi a = .164$ or $\kappa = .1687$ for $C_{sw} = 0$ and $m_\pi a = .244$ or $\kappa = .1428$ for $C_{sw} = 1.57$). As we discuss in this section, this improved analysis allows us to observe clearly the quenched chiral log effect in the pion mass with a value of the chiral log parameter δ slightly less than the previously established upper bound ($\delta = .054$) for the $C_{sw} = 0$ case. The value of δ is somewhat larger for clover improved quarks ($\delta = .073$), suggesting that the suppression of δ compared to the expected continuum value $\approx .17$ may be at least partially due to finite lattice spacing effects. The recent results from CPPACS of $\delta = .06 - .12$ [3] for several values of β is consistent with this possibility but is not accurate enough to observe any clear lattice spacing dependence.

To extract a value of the chiral log parameter from the pion mass as a function of bare quark mass, we shall consider in this section only the case where the two quark masses involved are equal (in Section 7 chiral log formulas for unequal quark masses will be derived from a model chiral Lagrangian and used to perform global fits to the b lattice data). In the equal quark mass case, the chiral logs sum up in a leading log approximation to give an

Table 2: Pseudoscalar masses and decay constants for $C_{sw} = 1.57$ (first four columns) and $C_{sw} = 0$ (last four columns) at $\beta = 5.7$.

κ	m_{Pa}	f_{Aa}	f_{Pa}	κ	m_{Pa}	f_{Aa}	f_{Pa}
.1400	.603(2)	.196(2)	.458(5)	.1610	.647(1)	.224(3)	.518(9)
.1405	.556(2)	.190(2)	.444(5)	.1630	.558(1)	.199(2)	.471(9)
.1410	.505(2)	.183(2)	.430(6)	.1650	.458(1)	.174(2)	.424(8)
.1415	.450(3)	.176(2)	.418(6)	.1667	.356(2)	.154(2)	.387(8)
.1420	.386(3)	.169(2)	.410(7)	.1675	.297(2)	.144(2)	.371(8)
.1423	.342(4)	.165(3)	.410(9)	.1680	.254(2)	.136(5)	.358(12)
.1425	.307(4)	.163(3)	.413(10)	.1683	.221(3)	.132(6)	.353(19)
.1427	.267(5)	.161(4)	.424(14)	.1685	.195(4)	.129(7)	.342(25)
.1428	.245(6)	.161(5)	.439(17)	.1687	.164(5)	.126(11)	.345(38)
κ_c	---	.151(2)	---	κ_c	---	.122(2)	---

anomalous power law dependence of the squared pion mass on the quark mass,

$$m_\pi^2 = \text{const.} \times m_q^{\frac{1}{1+\delta}} \quad (29)$$

For $C_{sw} = 1.57$ we calculated the pion mass at 9 values of hopping parameter ranging from $\kappa = .1400$ to $.1428$. The masses are obtained from a combined, correlated fit of smeared-local and smeared-smeared propagators, using a smeared pseudoscalar source, a local pseudoscalar source, and a local axial-vector source. The pion masses obtained are listed in Table 2.

Figures [12] and [13] exhibit the chiral log effect in the pseudoscalar mass graphically. The first plot includes all nine values of quark mass. The solid line is the best quadratic fit (i.e. $m_\pi^2 = Am_q + Bm_q^2$) to the four heaviest masses (with κ_c included as a fit parameter). The second plot (Fig[13]) is an expanded view of the small mass region. It shows clearly

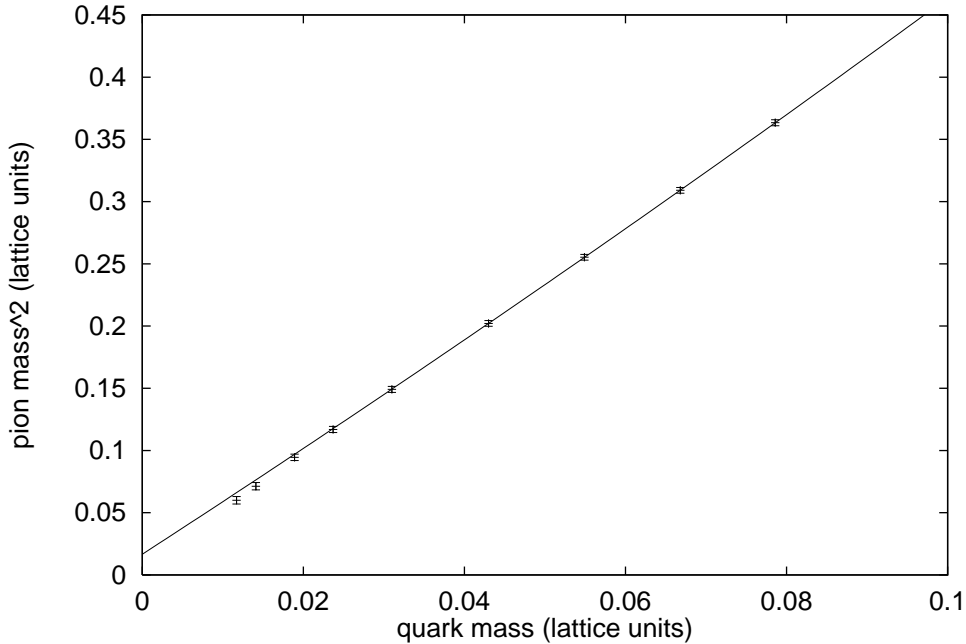


Figure 12: m_p^2 vs. quark mass for $\beta = 5.7$ and $C_{sw} = 1.57$. Solid line is the second order χPT fit to the four heaviest masses.

that the light pion masses fall below the quadratic extrapolation of the heavier masses (solid line). The dashed line is a fit of the lowest five masses to the chiral log formula (29) (again with the value of κ_c as one of the fit parameters). We find

$$\delta = .073(20) \tag{30}$$

We have also calculated the pion masses for $C_{sw} = 0$ on an ensemble of 200 gauge configurations at $\beta = 5.7$ on a $16^3 \times 32$ lattice (the “a” ensemble from the ACPMAPS library). Here also we calculate m_π at nine values of hopping parameter ranging from $\kappa = .1610$ to $\kappa = .1687$. For this case we were able to go to an even smaller pion mass of $m_\pi a = .164$ which is less than 200 MeV in physical units (using the charmonium scale $a^{-1} = 1.18$ GeV). The pion masses are listed in Table 2. Again the quenched chiral log effect is clearly visible, with the lightest-mass points falling significantly below an extrapolated

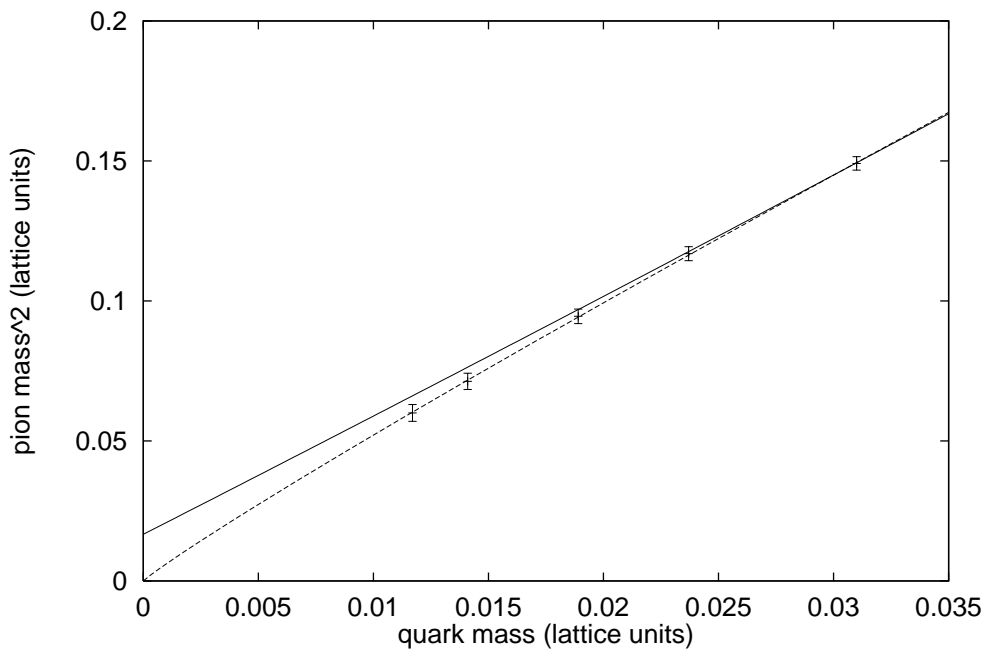


Figure 13: Quenched chiral log fit (dashed line) to the lightest 5 mass values with $\delta = .073$. Solid line is the extrapolated χPT fit to the heaviest four masses.

quadratic fit. Fitting to the quenched chiral log formula (29) we find

$$\delta = .054(20) \tag{31}$$

Consistent with the direct hairpin calculation, the value of the chiral log parameter from the m_π^2 analysis is somewhat smaller for $C_{sw} = 0$ than for $C_{sw} = 1.57$, although in this case the error bars are larger, so the difference is only marginally significant.

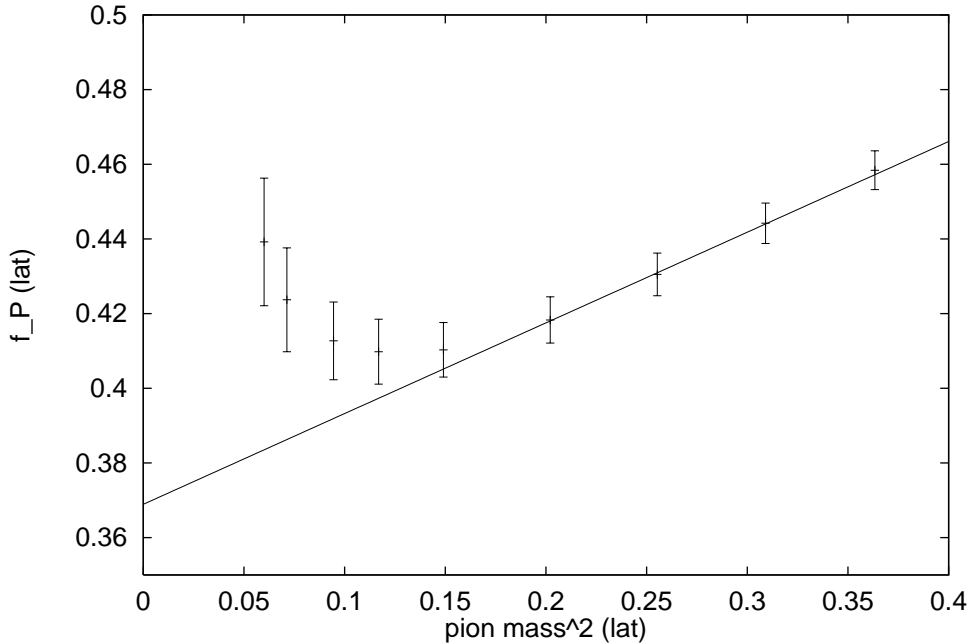


Figure 14: Pseudoscalar decay constant f_P as a function of quark mass. Enhancement at small m_q is a QCL effect.

6 Chiral behavior of the pseudoscalar and axial-vector matrix elements

As discussed in the Introduction, the chiral behavior of the pseudoscalar and axial-vector decay constants f_P and f_A provide further tests of quenched chiral log predictions. When the two quarks in the pseudoscalar meson have equal mass, we should find a clear contrast between these two quantities: f_P should exhibit a QCL factor $\propto (m_\pi^2)^{-\delta}$ while f_A should have a smooth, nonsingular chiral limit. The values of f_P and f_A are obtained from the combined fit to smeared-smeared and smeared-local propagators discussed in Section 5. The effects of full tadpole improvement for the normalization of quark masses and quark operators have been included in our calculations, but we have not carried out a complete nonperturbative $O(a)$ improvement program. The numerical results are presented in Table

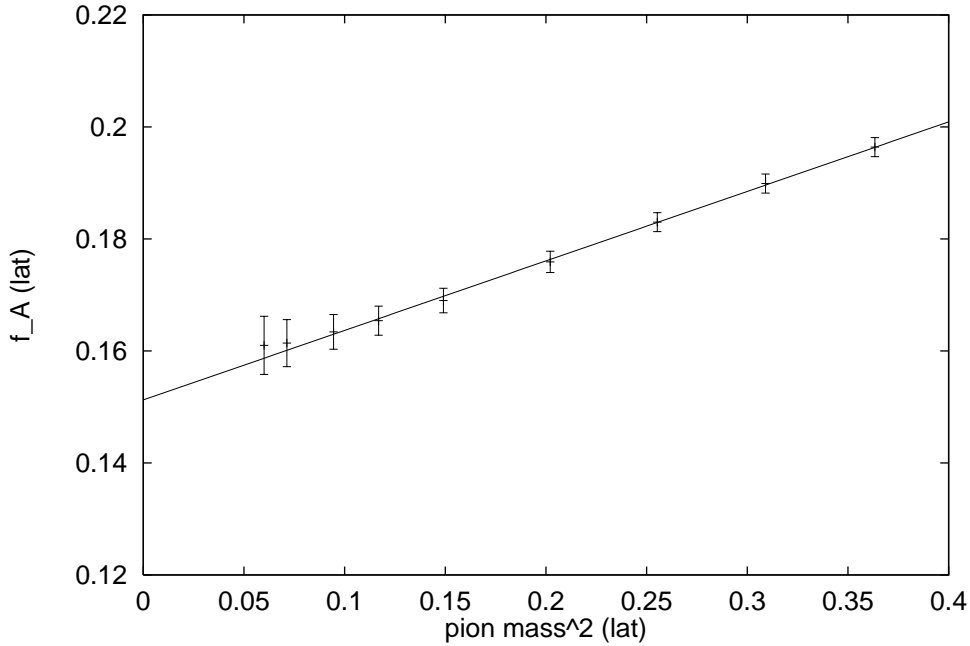


Figure 15: Axial-vector decay constant f_A as a function of quark mass. Note the absence of a QCL enhancement, as predicted by theoretical arguments.

2. For the $C_{sw} = 1.57$ results, the mass dependence of the decay constants is shown in Figures [14] and [15]. It is clear from these plots that at the very lightest masses, the value of f_P is significantly larger than a linear extrapolation of the heavier mass results, consistent with the singular $(m_\pi^2)^{-\delta}$ expected from QCL effects, while f_A exhibits no sign of singular behavior, and is well described by a linear fit. In both figures, the solid line is the best linear fit to the four heaviest masses.

Since the singular behavior of f_P in the chiral limit is determined by the ubiquitous chiral log parameter δ , it should be possible to use the results for f_P to obtain another estimate of this parameter. The extraction of a value of δ is made somewhat more difficult by the fact that, in addition to the singular QCL effect, the mass-dependence of f_P also has a significant contribution from higher order chiral perturbation theory (i.e. terms linear in m_π^2). With the accuracy of our data, the two contributions are difficult to disentangle.

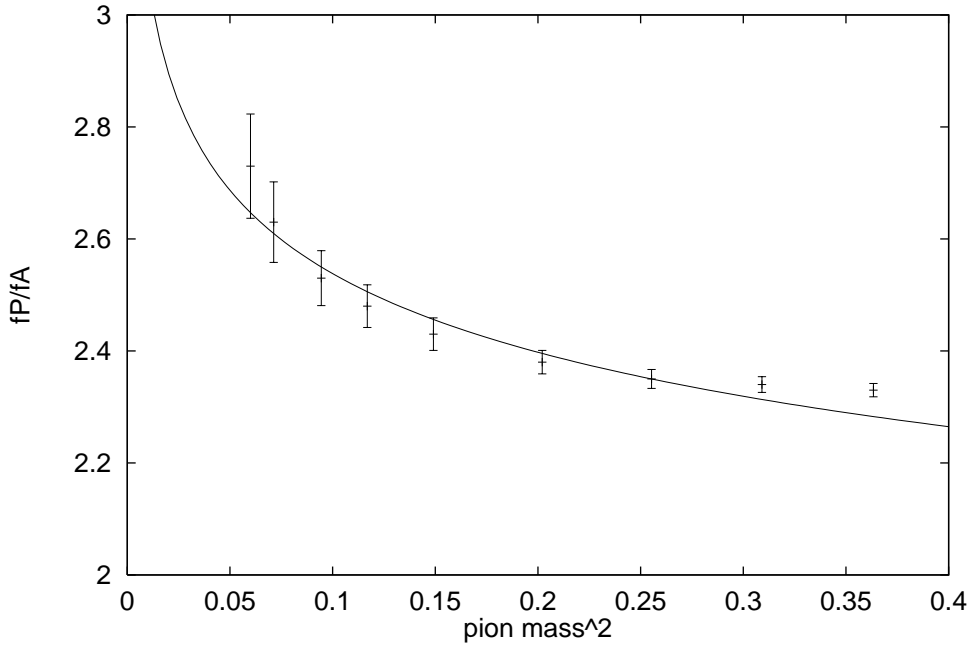


Figure 16: Ratio f_P/f_A as a function of quark mass. Solid line is a QCL fit with $\delta = .085$.

Although the QCL effect is clearly visible, a fit to f_P which includes both QCL terms and χPT terms is rather unstable and the resulting value for δ is poorly determined. We can do much better if we make an additional, phenomenologically motivated assumption that the perturbative slopes of f_P and f_A are approximately equal [14]. The data in Figures [14] and [15] are consistent with this assumption. The ratio f_P/f_A should thus exhibit a relatively pure chiral log behavior,

$$\frac{f_P}{f_A} = \text{const.} \times (m_\pi^2)^{-\delta} \quad (32)$$

The lattice results for this ratio are shown in Fig[16], along with the best fit to the QCL formula (32). This gives a value of the chiral log parameter of

$$\delta = .085(23) \quad (33)$$

7 Extraction of δ from mass and decay constant cross-ratios

To facilitate a comparison with previous work by the CPPACS collaboration [3], we have extracted the chiral log parameter δ from our full set of b-lattice clover-improved results for masses and decay constants of the 45 independent mesons which can be formed from the nine available quark masses, using the cross-ratio method introduced in [3]. For a given meson parameter y_{ij} (here i, j label the quarks in the meson and run from 1 to 9), the cross-ratio R_{ij} is defined as follows

$$R_{ij} \equiv \frac{y_{ij}^2}{y_{ii}y_{jj}} \quad (34)$$

Let M_{ij} , $f_{P;ij}$, and $f_{A;ij}$ denote the mass, pseudoscalar and axial-vector decay constant of the meson with quark content i, j (and quark masses m_i and m_j). Then, with either $y_{ij} = M_{ij}^2/(m_i + m_j)$ or $y_{ij} = \frac{f_{P;ij}}{f_{A;ij}}$, one has, to leading order in δ , *but ignoring higher order chiral perturbation theory contributions* (this amounts to setting $L_5, L_8 = 0$ in the chiral formulas (46,58,59) discussed in Section 8 below),

$$R_{ij} = \text{const.} \times (1 + \delta X_{ij}) \quad (35)$$

where the chiral logarithm is contained in the factor X_{ij} . At infinite volume, this factor becomes

$$X_{ij} = 2 + \frac{m_i + m_j}{m_i - m_j} \ln \frac{m_j}{m_i} \quad (36)$$

Our lattices are at smaller volume than those in the work cited above (physical extent $\simeq 2$ fermi as compared to 3 fermi in [3]) and we go to considerably smaller quark masses, so we have used a finite volume version of the fitting parameter X_{ij} (see Section 8 below for a discussion):

$$X_{ij} = 2I_{ij} - I_{ii} - I_{jj} \quad (37)$$

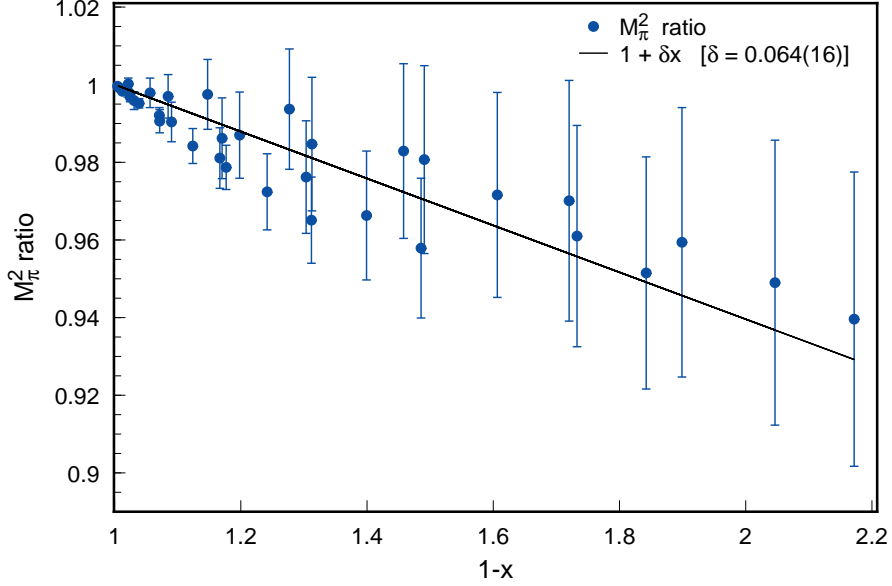


Figure 17: Cross-Ratios of $M_{ij}^2/(m_i + m_j)$ as a function of finite volume X_{ij} variable where the finite volume sums I_{ij} are defined in (44).

Fitting the cross-ratios of the masses of all 36 off-diagonal mesons, we obtain

$$\delta = 0.0604 \pm 0.0155 \quad (\chi^2 = 54/35 \text{ d.o.f}) \quad (38)$$

while a fit of cross-ratios of the decay constant ratios $\frac{f_{P;ij}}{f_{A;ij}}$ gives

$$\delta = 0.0708 \pm 0.0104 \quad (\chi^2 = 37/35 \text{ d.o.f}) \quad (39)$$

Finally, a combined fit of both the mass and decay-constant ratios gives

$$\delta = 0.0732 \pm 0.0081 \quad (\chi^2 = 118/71 \text{ d.o.f}) \quad (40)$$

The expected linearity in the X-variable of (35) is displayed graphically in Fig[17] for the pseudoscalar masses and in Fig[18] for the ratio of pseudoscalar to axial decay constants. The results of fully correlated fits are displayed as solid lines.

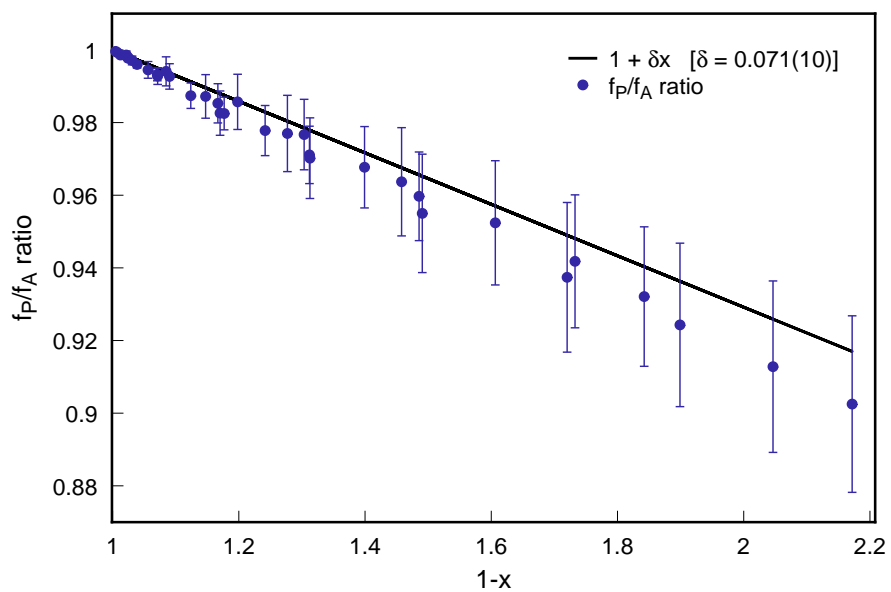


Figure 18: Cross-Ratios of $f_{P;ij}/f_{A;ij}$ as a function of finite volume X_{ij} variable

8 Comparison with quenched chiral perturbation theory

For pions made from a quark and antiquark with unequal masses, the form of the quenched chiral log effect is more complicated [3, 7]. For the range of masses we consider, it is sufficient to keep only lowest order terms in δ (i.e. one-loop terms), or equivalently, in a hairpin mass term which can be included explicitly as a correction to the basic chiral Lagrangian :

$$\begin{aligned}
\mathcal{L} &= \frac{f^2}{4} \text{Tr}(\partial_\mu U^\dagger \partial^\mu U) \\
&+ \frac{f^2}{4} \text{Tr}(\chi^\dagger U + U^\dagger \chi) + L_5 \text{Tr}(\partial_\mu U^\dagger \partial^\mu U (\chi^\dagger U + U^\dagger \chi)) \\
&+ L_8 \text{Tr}(\chi^\dagger U \chi^\dagger U + U^\dagger \chi U^\dagger \chi) + \mathcal{L}_{\text{hairpin}}
\end{aligned} \tag{41}$$

where

$$\mathcal{L}_{\text{hairpin}} \equiv -\frac{1}{2} m_0^2 \frac{f^2}{8} (i \text{Tr} \ln(U^\dagger) - i \text{Tr} \ln(U))^2 \tag{42}$$

The lowest order chiral Lagrangian has been supplemented by the chiral symmetry breaking terms L_5 of $\mathcal{O}(p^2 m_\pi^2)$ and L_8 of $\mathcal{O}(m_\pi^4)$ which model the leading mass-dependence of the slope in the pseudoscalar masses. Starting from this Lagrangian, we can derive explicit formulas for the pseudoscalar masses, and pseudoscalar and axial vector decay constants, consistent through order p^4 and including the effects of the hairpin mass insertion (assumed local) through the term $\mathcal{L}_{\text{hairpin}}$ in (41). The coefficients L_5, L_8 follow the notation of Gasser and Leutwyler [14]. The evaluation of the one loop chiral integrals appearing in this calculation has also been carried out at finite volume (appropriate for the physical size of the lattices used), and with a Pauli-Villars subtraction to regulate the ultraviolet. For example, logarithmically divergent integrals such as

$$I_{ij} = \frac{1}{\pi^2} \int d^4 p \frac{1}{p^2 + M_i^2} \frac{1}{p^2 + M_j^2} \tag{43}$$

are replaced by

$$I_{ij} = 16\pi^2 \sum_p (D(p, M_i)D(p, M_j) - D(p, \Lambda)^2) \quad (44)$$

where the momentum integration is now a discrete sum over a finite volume free boson propagator $D(p, M)$. We have typically chosen the cutoff scale $\Lambda \simeq \frac{1}{a}$ but sensitivity of the results to this choice is very small. One also encounters quadratically divergent graphs in the course of the calculation, which are regulated as follows:

$$I_i = 16\pi^2 \sum_p (D(p, M_i) - D(p, \Lambda) - (\Lambda^2 - M_i^2)D(p, \Lambda)^2) \quad (45)$$

With these preliminaries, we find the following expression for the pseudoscalar masses (squared), up to first order in the hairpin mass and (independently) in L_5 and L_8 :

$$\begin{aligned} M_{ij}^2 &= \frac{\chi_i + \chi_j}{2} (1 + \delta I_{ij}) \times \\ &\quad \left\{ 1 + \frac{1}{f^2} (8L_8 - 4L_5) (\chi_i + \chi_j) + \frac{1}{f^2} \delta (8L_8 - 4L_5) (2I_{ii}\chi_i + 2I_{jj}\chi_j + (\chi_i + \chi_j)I_{ij}) \right. \\ &\quad \left. + 8\frac{1}{f^2} L_5 \delta J_{ij} \right\} \end{aligned} \quad (46)$$

$$J_{ij} \equiv (I_i + I_j - (M_{ii}^2 + M_{jj}^2)I_{ij})/2 \quad (47)$$

The quantities χ_i encode the quark masses: our data includes values for 9 different kappa values, so the indices i, j above run from 1 to 9, allowing for 45 independent quark-antiquark combinations. Thus

$$\chi_i = 2r_0 m_i \quad (48)$$

where r_0 is a slope parameter (which we also extract from the fits) and we have used the pole value for the quark mass:

$$m_i \equiv \ln\left(1 + \frac{1}{2\kappa_i} - \frac{1}{2\kappa_c}\right) \quad (49)$$

Similar formulas were obtained for the pseudoscalar and axial decay constants $f_{P;ij}, f_{A;ij}$ and are listed in Appendix 2. We have performed global fits to the masses and decay constants for all 45 mesons in order to extract the parameters f, r_0, δ, L_5 and L_8 . The fits were performed for a variety of time-windows (for the $12^3 \times 24$ b lattices, on time windows 5-11, 6-11, 7-11 and 8-11) in order to isolate any remaining sensitivity to higher state contamination, and the results for the various chiral parameters, as a function of the initial time for the window, are shown in Fig[19]. With only 300 independent configurations, it is not possible to obtain a sufficiently stable covariance matrix to fit all 135 masses and decay constants, so these results reflect an uncorrelated fit to all meson parameters using (46), (58) and (59).

To summarize our results, a global fit to all pseudoscalar masses and decay constants, using a time window of 6-11, gives a final value for the chiral log parameter of

$$\delta = 0.059 \pm 0.015 \quad (50)$$

while the slope and critical kappa parameters in (48,49) are determined as

$$r_0 = 1.99 \pm 0.12 \quad (51)$$

$$\kappa_c = 0.143287 \pm 0.000022 \quad (52)$$

For the chiral breaking parameters L_5 and L_8 , our fits give

$$L_5 = (2.5 \pm 0.5) \times 10^{-3} \quad (53)$$

and

$$L_8 - \frac{1}{2}L_5 = (0.2 \pm 0.1) \times 10^{-3} \quad (54)$$

The dimensionless chiral parameters L_5, L_8 are only roughly determined by phenomenology. Recent estimates [17] give

$$L_5(M_\rho) = (1.4 \pm 0.5) \times 10^{-3} \quad (55)$$

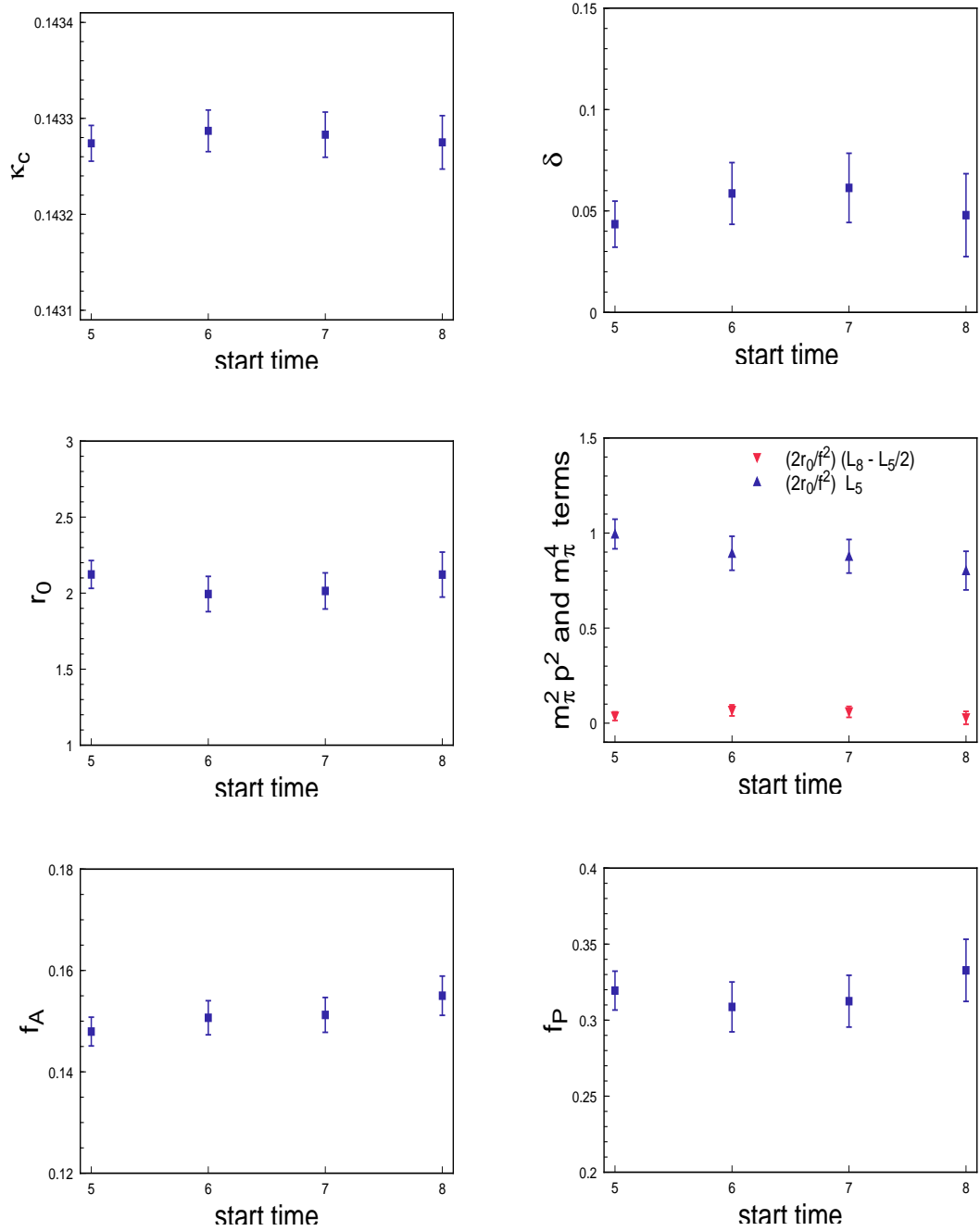


Figure 19: Global Fits, using (46,58,59), for $\kappa_C, \delta, r_0, L_{5,8}, f_A = \sqrt{2}f,$ and $f_P = r_0 f_A.$ Results are shown for time windows 5-11,6-11,7-11, and 8-11

renormalized at the rho mass, with the combination $L_8 - \frac{1}{2}L_5$ consistent with zero:

$$L_8 - \frac{1}{2}L_5 = (0.2 \pm 0.4) \times 10^{-3} \quad (56)$$

Finally, our result for the axial decay constant corresponds to a value for the pion decay constant (bare, in lattice units) of

$$f = f_\pi = 0.1066 \pm 0.0024 \quad (57)$$

9 Summary and discussion

The calculations presented above confirm all the essential features of anomalous quenched chiral behavior suggested by continuum calculations. Our lattice studies lead to the following basic conclusions:

1. The MQA pole-shifting technique allows for accurate computation of meson and hairpin correlators down to small quark masses ($M_\pi < 200$ MeV). Probing this region is essential in order to obtain reliable signatures of anomalous chiral behavior.
2. The hairpin vertex has only a small coupling to excited states, and very gentle momentum dependence. This suggests that it may be accurately modelled by a local mass-insertion term in a chiral Lagrangian.
3. Determination of the chiral log parameter δ using five separate methods gives consistent results. A summary of our results for this parameter indicating the various methods used is displayed in Table 3. The overall average of our $C_{sw} = 1.57$ methods gives $\delta = 0.065 \pm 0.013$. Our values for δ at $\beta = 5.7$ are considerably smaller than those expected from a naive continuum analysis, but are in agreement with previous lattice estimates.
4. Using the MQA technique, meson properties (masses and decay constants) can be extracted with sufficient accuracy to allow a fit of higher order chiral parameters, such as L_5 and L_8 .

Careful quantitative studies of chiral behavior in quenched QCD in comparison to quenched chiral perturbation theory can provide a great deal of insight into the connection between QCD and the effective chiral Lagrangian that describes its long range behavior in the limit of small quark mass. Even if the numerical simulation of full QCD were not so

Table 3: Summary of results for chiral log parameter δ

Method	C_{sw}	δ
Witten-Veneziano	1.57	0.063(6)
hairpin vertex	1.57	0.062(7)
diagonal mesons	1.57	0.073(20)
ratio fit, masses	1.57	0.060(16)
ratio fit, f_P/f_A	1.57	0.071(10)
global fit	1.57	0.059(15)
Witten-Veneziano	0	0.074(9)
hairpin vertex	0	0.044(5)
diagonal mesons	0	0.054(20)

expensive computationally, the study of chiral behavior in quenched QCD would still be of theoretical interest. For example, the Witten-Veneziano relation connects the η' mass to the topological susceptibility of *quenched* QCD. The geometric summation of multiple η' mass insertions is only the simplest example of how, in some cases, the most important effects of the full QCD fermion determinant can be incorporated into a quenched result, with the guidance of chiral perturbation theory. Because of the smallness of the parameter δ , QCL effects are adequately described by one-loop χ PT, even for quark masses close to the physical up and down mass. It is thus straightforward to apply appropriate and calculable QCL corrections to quenched results. Of course the masses, decay constants, and higher order chiral Lagrangian coefficients obtained in quenched QCD will differ somewhat from those of the full theory, but all of the disturbing structural properties of the quenched theory (lack of unitarity, absence of topological screening, etc.) can be systematically repaired in the context of chiral perturbation theory. Further precision studies of anomalous chiral

behavior in the quenched meson and baryon spectrum should provide additional insight into the origin and structure of chiral symmetry in QCD. The results presented in this paper provide strong support for the usefulness of the MQA technique to facilitate these studies.

Ideally, similar studies should be performed using an exactly chirally symmetric Dirac operator which satisfies Ginsparg-Wilson relations, e.g. the Neuberger operator[15]. Explicit Ginsparg-Wilson chiral symmetry would resolve the exceptional configuration problem *ab initio*. Unfortunately, such operators are necessarily not ultralocal[16], and are difficult to invert or diagonalize numerically.

The MQA method attempts to account for the most salutary effect of an explicitly chirally symmetric approach. The underlying assumption in this procedure is that the most important effect of the explicit chiral symmetry breaking contained in the Wilson-Dirac operator is the real displacement of its small eigenvalues. The MQA method merely removes these displacements in a compensated manner. The principal disadvantage of the method is its apparent lack of locality. Using a basis of hopping terms (nearest-neighbor, next-nearest neighbor, etc.), it may be possible to identify terms in an ultralocal expansion of the Dirac operator which correspond most closely to an MQA improved Wilson-Dirac operator. The additional hopping terms would have the effect of reducing the dispersion of the small real eigenvalues as well as inducing small rotations of the basis wavefunctions, etc. Such an analysis has not been carried out yet. The clear quantitative success of the MQA procedure in restoring desired chiral behavior is a promising indication that such eigenmode-based methods can be both efficient and effective in removing the dominant spurious effects of chiral symmetry breaking contained in the Wilson-Dirac formulation of lattice fermions.

Appendix 1: The allsource method

The allsource method, first applied to the η' mass calculation in Ref. [11], is used here to calculate hairpin diagrams as well as the pseudoscalar charge for the determination of winding numbers. We have also introduced a generalization of this allsource method which allows the calculation of closed loops which originate from a smeared source, i.e. the two ends of the quark propagator are contracted over color and spin, but are spatially separated with an exponential weight function. The method relies on the fact that gauge noninvariant terms in the calculation will cancel out due to random $SU(3)$ gauge phases. For example, in the calculation of a single quark loop, the closed loop terms where the quark starts and ends on the same point (or on the same exponential source in the smeared calculation) add coherently when summed over sites, while loops which start and end on different sources have random phases and cancel.

While the cancellation of random gauge phases in the allsource method should work arbitrarily well for a large enough ensemble of gauge configurations, it is very instructive to test this method in a situation where we know the exact gauge invariant answer which can be used to check the accuracy of the random phase cancellation. To carry out such a comparison, we have calculated the ordinary valence pion propagator using the allsource technique. This calculation uses the same allsource propagators that were used to calculate hairpin correlators. In the hairpin calculation, we computed the correlator of two closed loops by contracting the two color indices of each allsource propagator with a fixed time separation between the two propagators. To calculate the valence propagator, we instead take the same two allsource propagators with fixed time separation and cross-contract the color indices to form a single loop from the two propagators and then project out the color singlet component. (The last step amounts to leaving out the terms in which all four color indices are equal and then multiplying by a factor of $3/2$.) In Fig[20], the valence pion

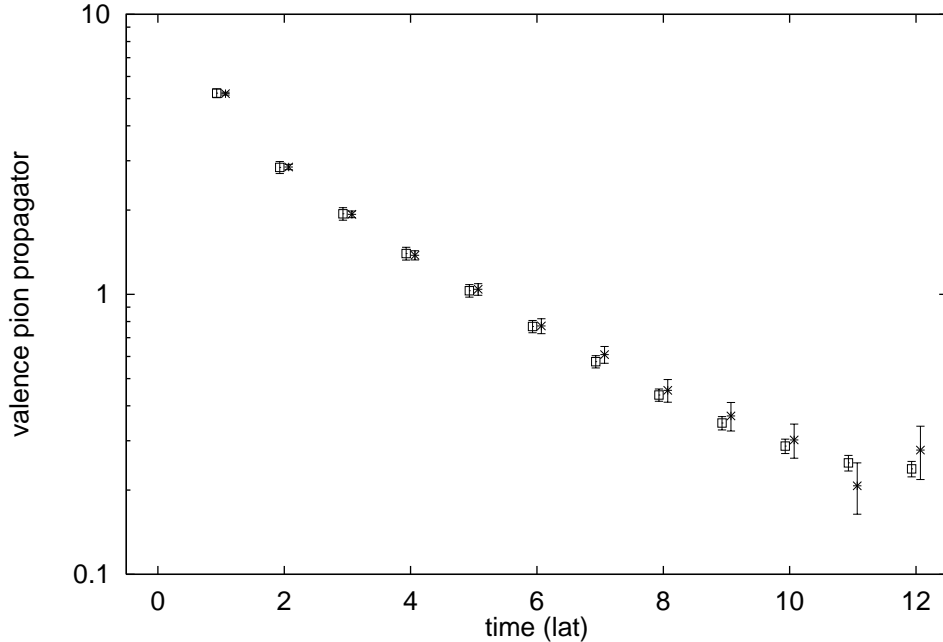


Figure 20: Comparison of valence pion propagator computed by allsource method (\times 's) and conventional method (boxes). Data points are offset slightly for clarity.

propagator calculated by the allsource method is compared with the results of the standard calculation using local and smeared sources on a fixed timeslice. The results are shown for hopping parameter $\kappa = .1425$, but similar agreement is obtained at all kappa values.

The agreement is excellent and well within statistical errors. For small times ($t < 5$), the errors on the allsource calculation are actually smaller than those from a fixed source. (Remember that the allsource calculation allows the meson propagator to be averaged over all locations on the lattice, thus increasing the effective statistics relative to the fixed source method.) Unlike the fixed source calculation however, the statistical errors for the allsource calculation are more-or-less constant in absolute magnitude for all time separations. This results in a signal-to-noise ratio that gets rapidly worse as we go out in time, just as in the hairpin calculation. This roughly constant noise level is presumably the effect of incomplete cancellation of random gauge phases. Because of this, the allsource method is an inferior way of studying the asymptotic behavior of the pion propagator. Nevertheless, for short times it accurately reproduces the results of the standard method. It is a fortuitous circumstance

that the hairpin correlator is found to be almost entirely free of excited state contamination. This allows us to extract the ground state vertex insertion from its value at relatively short times where the allsource technique is accurate.

Appendix 2: Quenched chiral results for decay constants

A next to leading order chiral perturbation theory calculation of the pseudoscalar and axial decay constants can be carried out along the same lines as discussed in Section 8 for the pseudoscalar mass spectrum. Starting from the Lagrangian (41) and using the notations introduced there, we find

$$\begin{aligned}
f_{P;ij} &= \sqrt{2}fr_0(1 + \frac{1}{4}\delta(I_{ii} + I_{jj} + 2I_{ij})) \times \\
&\{ 1 + \frac{1}{f^2}(8L_8 - 2L_5)(\chi_i + \chi_j)(1 + \delta(2I_{ii}\chi_i + 2I_{jj}\chi_j + (\chi_i + \chi_j)I_{ij}))/(\chi_i + \chi_j) \\
&- \frac{2}{f^2}L_5\delta(I_{ii}\chi_i + I_{jj}\chi_j + (\chi_i + \chi_j)I_{ij}) \\
&+ \frac{4}{f^2}L_5\delta(J_{ii} + J_{jj})\}
\end{aligned} \tag{58}$$

for the pseudoscalar decay constant, and

$$\begin{aligned}
f_{A;ij} &= \sqrt{2}f(1 + \frac{1}{4}\delta(I_{ii} + I_{jj} - 2I_{ij})) \times \\
&\{ 1 + \frac{2}{f^2}L_5(\chi_i + \chi_j) + 2\frac{1}{f^2}L_5\delta(2(\chi_i + \chi_j)I_{ij} - \chi_i I_{ii} - \chi_j I_{jj})\}
\end{aligned} \tag{59}$$

for the axial decay constant. These formulas, together with

$$\begin{aligned}
M_{ij}^2 &= \frac{\chi_i + \chi_j}{2}(1 + \delta I_{ij}) \times \\
&\{1 + \frac{1}{f^2}(8L_8 - 4L_5)(\chi_i + \chi_j) + \frac{1}{f^2}\delta(8L_8 - 4L_5)(2I_{ii}\chi_i + 2I_{jj}\chi_j + (\chi_i + \chi_j)I_{ij}) \\
&+ 8\frac{1}{f^2}L_5\delta J_{ij}\}
\end{aligned} \tag{60}$$

for the pseudoscalar masses, were used to perform the global fits described in Section 8.

Acknowledgements

The work of W. Bardeen and E. Eichten was performed at the Fermi National Accelerator Laboratory, which is operated by University Research Association, Inc., under contract DE-AC02-76CHO3000. The work of A. Duncan was supported in part by NSF grant PHY97-22097. The work of H. Thacker was supported in part by the Department of Energy under grant DE-FG02-97ER41027.

References

- [1] W. Bardeen, A. Duncan, E. Eichten, and H. Thacker, Phys. Rev. D59 (1999) 014507.
- [2] W. Bardeen, A. Duncan, E. Eichten, G. Hockney and H. Thacker, Phys. Rev. D57 (1998) 1633.
- [3] S. Aoki et al, Phys. Rev. Lett.84 (2000) 238.
- [4] A. Duncan, E. Eichten, S. Perrucci and H. Thacker, Nucl. Phys. B (proc. Suppl.) 53 (1997) 256.
- [5] E. Witten, Nucl. Phys. B156 (1979) 269; G. Veneziano, Nucl. Phys. B159 (1979) 213.
- [6] S. Sharpe, Phys. Rev. D46 (1992) 3146.
- [7] C. Bernard and M. Golterman, Phys. Rev. D46 (1992) 853.
- [8] J. Smit and J. Vink, Nucl. Phys. B286 (1994) 485.
- [9] See for example, G.H. Golub and C.F. Van Loan, *Matrix Computations*, 2nd edition (Johns Hopkins, 1990).
- [10] J. W. McCune (unpublished).

- [11] Y. Kuramashi et al, Phys. Rev. Lett. 72 (1994) 3448.
- [12] L. Venkataraman and G. Kilcup, hep-lat/9711006.
- [13] F. Butler, H. Chen, J. Sexton, A. Vaccarino, and D. Weingarten, Nucl. Phys. B430 (1994) 179.
- [14] J. Gasser and H. Leutwyler, Nucl. Phys. B250 (1985) 465.
- [15] H. Neuberger, Phys. Lett. B437 (1998) 117.
- [16] I. Horvath, Phys. Rev. D60 (1999) 034510.
- [17] A. Pich, Rep. Prog. Phys. 58 (1995) 563-609.